electronics

Article

Energy Flow Analysis of Excavator System Based on Typical Working Condition Load

Deying Su, Liang Hou, Shaojie Wang *, Xiangjian Bu and Xiaosong Xia

Department of Mechanical and Electrical Engineering, Xiamen University, Xiamen 361000, China; 19920190154058@stu.xmu.edu.cn (D.S.); hliang@xmu.edu.cn (L.H.); bxj@xmu.edu.cn (X.B.); 19920200156022@stu.xmu.edu.cn (X.X.)
* Correspondence: wsj@xmu.edu.cn

Abstract: Accurate energy flow results are the premise of excavator energy-saving control research. Only through an accurate energy flow analysis based on operating data can a practical excavator energy-saving control scheme be proposed. In order to obtain the excavator's accurate energy flow, the excavator components' performance and operating data requirements are obtained, and the experimental schemes are designed to collect it under typical working conditions. The typical working condition load is reconstructed based on wavelet decomposition, harmonic function, and theoretical weighting methods. This paper analyzes the excavator system's energy flow under the typical working condition load. In operation conditions, the output energy of the engine only accounts for 50.21% of the engine's fuel energy, and the actuation and the swing system account for 9.33% and 4%, respectively. In transportation conditions, the output energy of the engine only accounts for 49.80% of the engine's fuel energy, and the torque converter efficiency loss and excavator driving energy account for 15.09% and 17.98%, respectively. The research results show that the energy flow analysis method based on typical working condition load can accurately obtain each excavator component's energy margin, which provides a basis for designing energy-saving schemes and control strategies.

Keywords: excavator; typical working condition; load; operating data; energy flow

Citation: Su, D.; Hou, L.; Wang, S.; Bu, X.; Xia, X. Energy Flow Analysis of Excavator System Based on Typical Working Condition Load. *Electronics* **2022**, *11*, 1987. https://doi.org/10.3390/electronics11131987

Academic Editors: Darius Andriukaitis, Yongjun Pan and Peter Brida

Received: 15 May 2022
Accepted: 23 June 2022
Published: 24 June 2022

1. Introduction

Excavators are commonly used in farmland water conservancy, urban greening and construction projects and are the construction machinery with the largest fuel consumption [1–3]. The engine output energy is converted into hydraulic energy or vehicle driving energy during the excavator's working process. Due to the significant mass attribute and the characteristics of multi-mechanism linkage, the excavator energy consumption is much higher than the actual working load. With the aggravation of the global energy crisis, air quality problems, and the tightening of construction machinery emission policies and regulations in various countries, many scholars have undertaken a large number of studies on the energy-saving control of excavators.

Yang et al. improved excavator engine efficiency through engine deactivation technology [4]. Researchers and major manufacturers worldwide have carried out a series of studies on hydraulic system control methods such as a load sensing (LS) system [5], negative flow system (NFS) [6], positive flow system (PFS) [7], and independent metering valve (IMV) [8], which effectively improved the excavator system efficiency. Kim and Zhao et al. researched boom gravitational potential energy and swing system energy recovery, respectively [9–11]. Xiao and Kwon researched the gas–electric hybrid excavator [12,13], and Shen studied the hybrid hydraulic excavator based on the accumulator [14,15]. Zimmerman and Paolo et al. established a mathematical model of the excavator system on simulation platforms MATLAB-Simulink and AMESim, respectively [16–18]. Based on the mathematical model, they realized the energy flow analysis of the excavator system and designed a hybrid excavator scheme [19,20]. In the above studies, simple signals such as constants, steps, and ramps are often used to simulate the working load, which are difficult to accurately represent the actual working condition, which will inevitably lead to deviations in the results of energy flow analysis and the effect of energy-saving schemes. In response to this problem, An et al. proposed an excavator energy flow analysis method based on operating data [21], but the study did not involve the construction of typical working condition load and could not be further applied to mathematical models. Therefore, it is urgent to build up the typical working condition load of the excavator, realize the accurate analysis of the energy flow, obtain the energy margin of the excavator system, and provide accurate simulation load for the mathematical model.

Zhai et al. compiled a load spectrum for hydraulic pump fatigue analysis based on the mixed distribution method [22,23], which focuses on the frequency of load action and cannot be applied to the energy flow analysis of excavators. Chang et al. use the theoretical weighted method to construct the typical working condition load of the loader [24], which ignored the non-stationary characteristics of the random term of the load. Based on the wavelet decomposition method, Wang obtained the swing condition load's random term and trend term, and the swing condition load function composed of the random term and the trend term function [25,26]. This study does not involve the load's reconstruction of the excavator's complete working condition, and it is not easy to achieve parametric characterization of the operation load of the main pump or other components. Based on the above analysis, this paper combines the wavelet decomposition method and the theoretical weighting method to construct the excavator's typical working condition load. The energy flow of the excavator system is analyzed based on typical working condition load, and an accurate energy margin is provided for the excavator system's energy-saving scheme.

The rest of the paper is organized as follows: Section 2 conducts a theoretical energy flow analysis of the excavator, Section 3 obtains component performance and operating data, Section 4 constructs the typical working condition load and analyzes the energy flow of the excavator, and Section 5 is a discussion of the results and gives conclusions.

2. Theoretical Energy Flow Analysis of Excavator System

The research objective of this paper is a wheel excavator, and its work system is shown in Figure 1, which consists of an engine, transmission system, and hydraulic system. The transmission system includes a hydraulic torque converter, front and rear drive axles, transmission shaft, etc. The hydraulic system consists of the main pump, steering pump, main control valve (MCV), actuators and swing motor, etc. Transportation and operation conditions are typical conditions of wheel excavators. The operation conditions are divided into five stages: dig preparation, digging, lifting, unloading, and swinging [27], as shown in Figure 2. Under transportation conditions, engine energy is converted into driving energy. In operation conditions, the engine leads the hydraulic pump to work through the coupling, and the main control valve distributes the flow rate of the hydraulic pump to the actuator, such as the boom, stick, bucket, and swing motor. There is no steering action during the wheel excavator's operation, and the steering pump's output flow rate is distributed to the swing system and the bucket mechanism by the main control valve. Except for the mode of transportation, wheel excavators are no different from crawler excavators, which will be referred to as excavators.

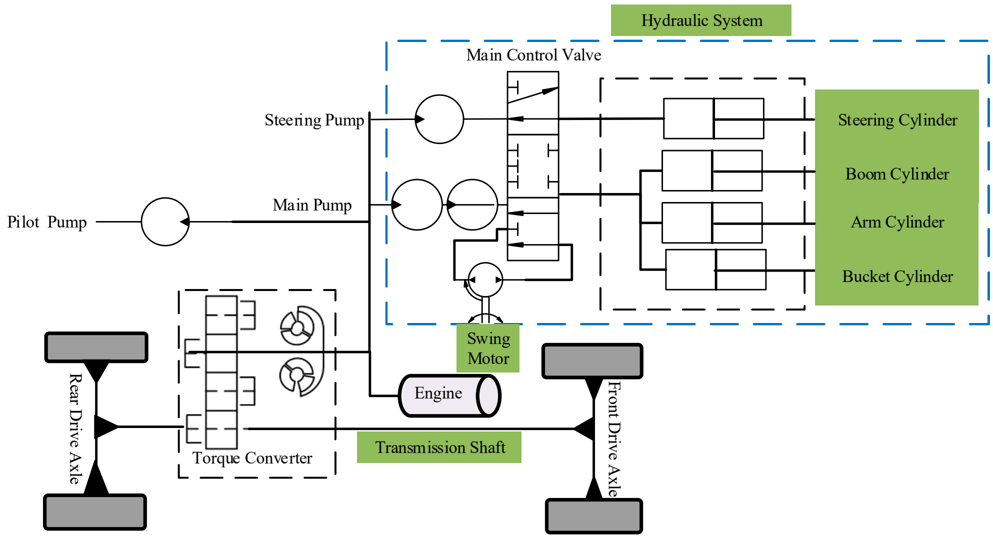

Figure 1. Excavator work system.

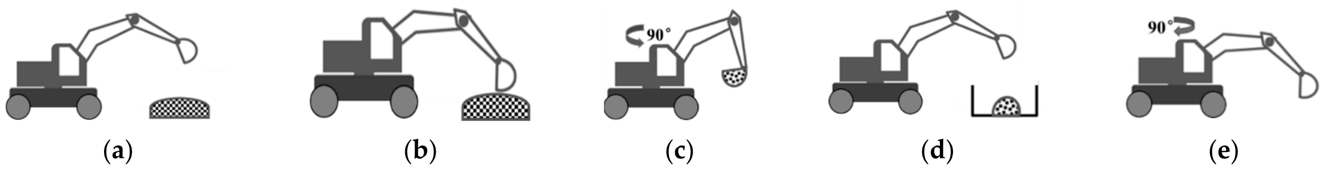

Figure 2. Operation stages of excavator. (**a**) Dig preparation; (**b**) digging; (**c**) lifting; (**d**) unloading; (**e**) swinging.

2.1. Engine Theoretical Energy Flow

The engine's energy transfer process includes heat loss, cylinder loss, mechanical friction loss, generator consumption, etc. The remaining output energy is transferred to the work system, and the theoretical energy flow is shown in Figure 3. The output energy is related to the output torque and speed, obtained by Equation (1). The heat loss is associated with the coolant temperature change and specific heat capacity, expressed by Equation (2). Cylinder loss, mechanical friction loss, and alternator consumption are expressed as other consumption by Equation (3). Finally, the theoretical energy flow of the engine is calculated by Equations (1)–(3).

$$P_{E\_outputenergy} = \frac{n \times M}{9549} \tag{1}$$

$$P_{E\_heatloss} = C_e \rho_e q_e \Delta\theta_e \tag{2}$$

$$P_{E\_otherconsumption} = mQ - P_{E\_outputenergy} - P_{E\_heatloss} \tag{3}$$

where m is the engine fuel quality, kg/s; Q is the fuel calorific value, J/kg; n is the engine output speed, rpm; M is the engine output torque, Nm; C_e is the coolant specific heat capacity, J/(kg °C); ρ_e is the coolant density, kg/m^3; q_e is the coolant flow rate, m^3/s; $\Delta\theta_e$ is the coolant temperature difference, °C.

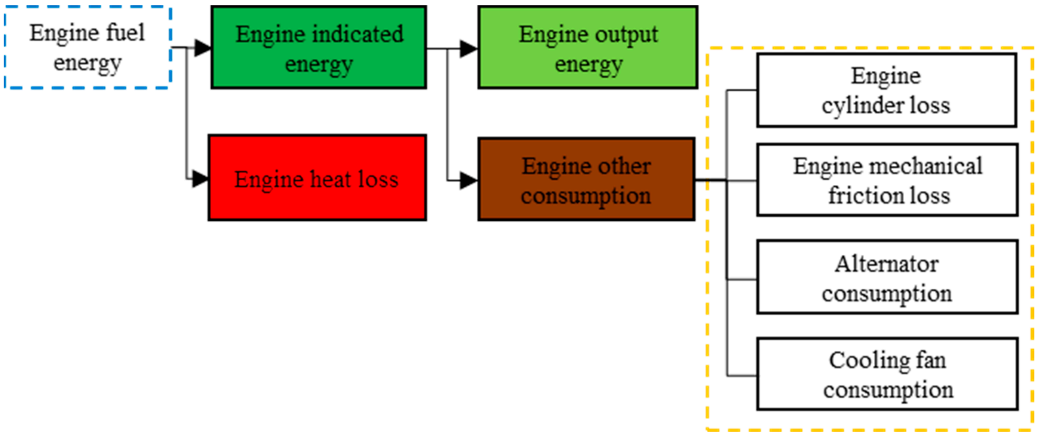

Figure 3. Engine energy flow.

2.2. Hydraulic Pump Theoretical Energy Flow

The engine's output energy is transmitted to the main pump, steering pump, and auxiliary components such as the cooling pump and the oil pump. The energy loss of the hydraulic pumps includes the efficiency loss and the hydraulic system's heat loss. The hydraulic pumps' energy flow is shown in Figure 4. According to the calculation method of hydraulic pump energy and the hydraulic system heat loss, the hydraulic pumps' energy flow is expressed by Equations (4)–(7).

$$P_{C\&O\_consumption} = P_{E\_outputenergy} - P_{P\_efficiencyloss} - P_{Hy\_heatloss} - P_{P\_outputenergy} \tag{4}$$

$$P_{P\_efficiencyloss} = \sum_{i=1}^{3} (1 - \eta_{hi}) P_{Pumpi} \tag{5}$$

$$P_{Pumpi} = \frac{P_i q_i}{60} \tag{6}$$

$$P_{Hy\_heatloss} = C_h \rho_h q_h \Delta\theta_h \tag{7}$$

where η_{hi} is the main pump 1, main pump 2, and steering pump efficiency; P_i is the main pump 1, main pump 2, and steering pump output pressure, bar; q_i is the main pump 1, main pump 2, and steering pump output flow rate, L/min; C_h, ρ_h, $\Delta\theta_h$ is the hydraulic oil specific heat capacity, density, and temperature difference, respectively, J/(kg·°C), kg/m^3, °C; q_h is the hydraulic oil flow rate, m^3/s.

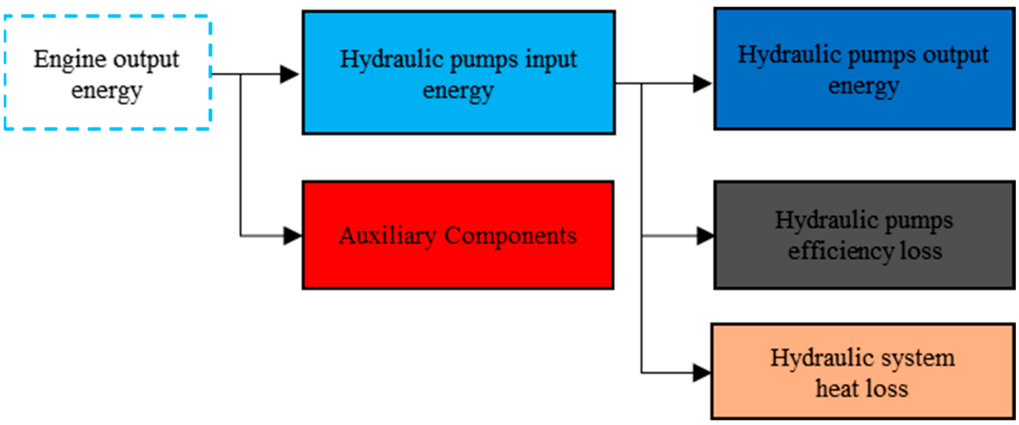

Figure 4. Excavator pump energy flow.

2.3. Operation System Theoretical Energy Flow

The energy flow of the excavator operation system is illustrated in Figure 5. The output energy of the hydraulic pump is transmitted to the actuation system and the swing motor through the MCV. The actuation system energy includes the boom energy, the stick energy, and the bucket energy. The operation system's loss includes the MCV loss, the hydraulic circuit loss, the cylinder loss, and overflow loss during the swing. Finally, the energy flow of the operation system is expressed by Equations (8)–(11).

$$P_{Actuator} = P_{boom} + P_{arm} + P_{bucket} \tag{8}$$

$$P_{System\_loss} = P_{Contralvalve\_inputenergy} - P_{Actuatorsystem} - P_{Swingmotor} \tag{9}$$

$$P_{Swingmotor} = P_{motorin} q_{motorin} \tag{10}$$

$$P_{Cylinder} = P_{in} q_{in} - P_{out} q_{out} \tag{11}$$

where $P_{motorin}$ is the motor inlet pressure, bar; $q_{motorin}$ is the motor inlet flow, L/min; P_{in} is the cylinder inlet pressure, bar; q_{in} is the cylinder inlet flow, L/min; P_{out} is the cylinder outlet pressure, bar; q_{out} is the cylinder outlet flow, L/min.

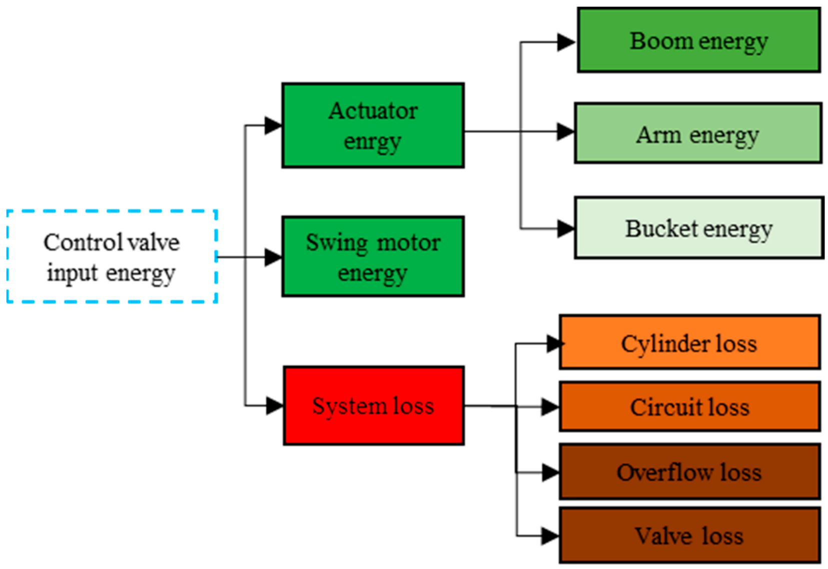

Figure 5. Excavator operation system energy flow.

2.4. Excavator System Theoretical Energy Flow under Transportation Condition

In the excavator transportation condition, the engine's output energy is sequentially transmitted to the transmission shaft, the drive axle, and the wheel reducer through the hydraulic torque converter, and finally, drive the excavator. The actuation system does not work during this period, and the main pump consumes the engine energy at the lowest output flow rate. The excavator energy flow under the transportation condition is shown in Figure 6. Depending on the calculation method of the theoretical energy flow and the tractive force [28], the energy flow in the transportation condition is expressed by Equations (12)–(16).

$$P_{Transmissionsystem} = P_{E\_outputenergy} - P_{Mainpunp\_loss} - P_{Steeringpump\_consumption} \tag{12}$$

$$P_{Excavator\_drivingenergy} = Fv \tag{13}$$

$$P_{T\_loss} = (1 - \eta_T) P_{Transmissionsystem} \tag{14}$$

$$F = \frac{M_{Out} \cdot i_T \cdot i_0 \cdot i_g \cdot \eta_T \cdot \eta_0 \cdot \eta_g}{1000 r_d} \tag{15}$$

$$v = 0.377 \frac{n_{Out} \cdot r_d}{i_T \cdot i_0 \cdot i_g} \quad (16)$$

where M_{Out}, n_{Out} are the output torque and speed of the torque converter, respectively; r_d is the radius of the wheel; η_T is the torque converter efficiency, which varies with speed and gear positions, and is measured by bench experiments; i_T, i_0, and i_g are the torque converter gear ratio, the total transmission ratio of drive shaft and front axle, and transmission ratio of the wheel reducer, respectively; η_0, η_g are the total efficiency of drive shaft and front axle, and the wheel reducer efficiency, which are taken as 0.9 and 0.8, respectively.

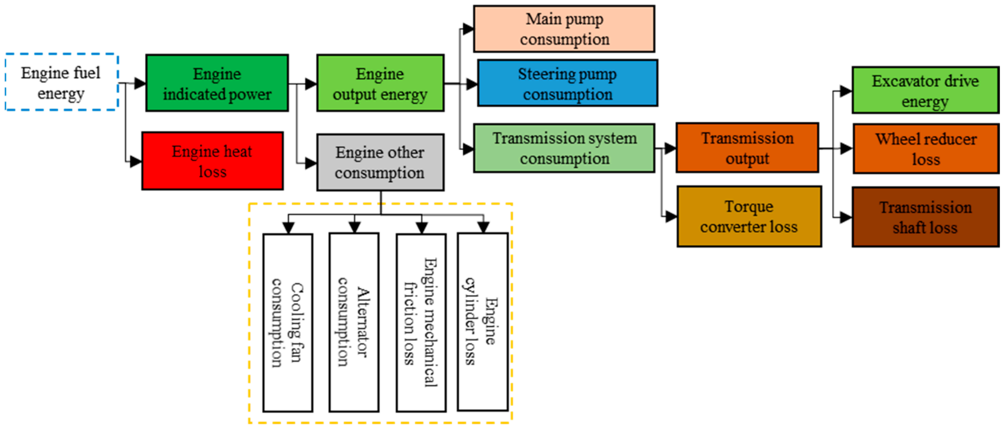

Figure 6. Excavator transportation condition energy flow.

Based on the above research, the energy flow analysis of the excavator system needs to obtain the component performance and operating data shown in Table 1. Operating data construct the typical working condition load, and the energy flow analysis is realized based on the typical working condition load and component performance parameters.

Table 1. Data requirements of components for the excavator energy flow analysis.

Serial Number	Components' Data	Serial Number	Components' Data
1	Engine fuel rate	16	Swing motor outlet pressure
2	Engine output torque	17	Swing motor inlet flow rate
3	Engine output speed	18	Swing motor outlet flow rate
4	Coolant temperature	19	Boom A chamber pressure
5	Coolant flow rate	20	Boom B chamber pressure
6	Main pump 1 pressure	21	Arm A chamber pressure
7	Main pump 1 flow rate	22	Arm B chamber pressure
8	Main pump 2 pressure	23	Bucket A chamber pressure
9	Main pump 2 flow rate	24	Bucket B chamber pressure
10	Steering pump pressure	25	Boom displacement
11	Steering pump flow rate	26	Arm displacement
12	Main pump 1 efficiency	27	Bucket displacement
13	Main pump 2 efficiency	28	Torque converter efficiency
14	Steering pump efficiency	29	Torque converter output speed
15	Swing motor inlet pressure	30	Torque converter output torque

3. Excavator Data Acquisition

3.1. Operating Data Acquisition

The data requirements of the excavator's components are obtained through the theoretical energy flow analysis. This section describes the operating data acquisition. The data types to be collected for components include speed, torque, temperature, pressure, flow rate, displacement, etc., as shown in Figure 7. The experiment requires that the operating data be collected and recorded stably and synchronously. The acquisition rate of the Dewe data acquisition system is 200 KS/s/ch, which can simultaneously collect analogue signals and digital signals. It has USB, CAN, GPS, video, and other data acquisition interfaces, and the data storage space is 500 GB, which can meet the requirements of this data acquisition.

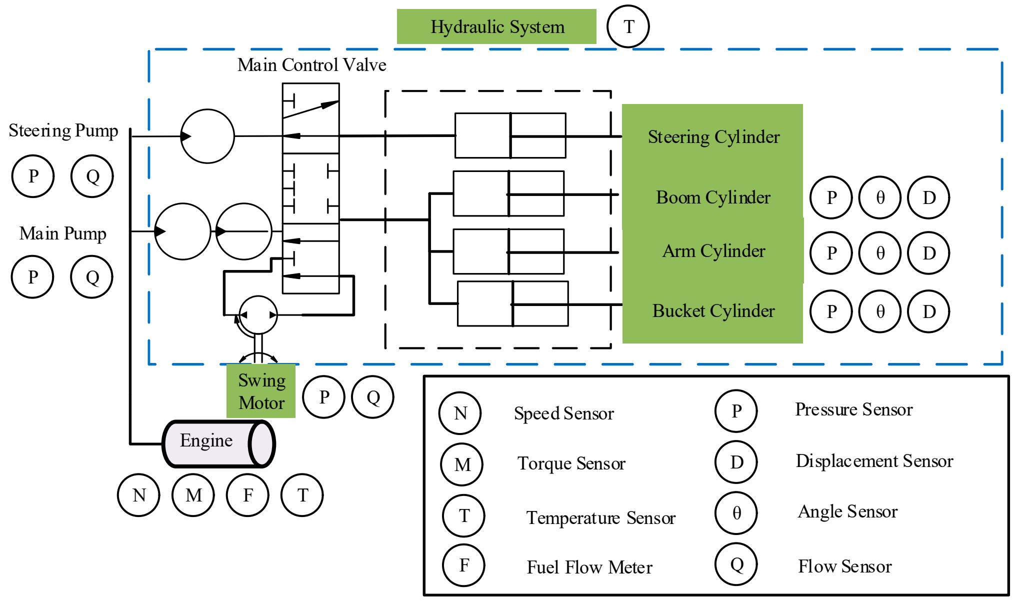

Figure 7. Data required for each component of excavator.

The excavator operation environment is very harsh, the flow sensor is expensive and easily damaged, and it is not easy to collect the flow rate data of the actuator through the flow sensor. In order to solve this problem, the cylinder pressure and displacement operating data are collected, and the cylinder's inlet and outlet flow rate is calculated through the cylinder dynamic relationship of Equations (17) and (18) [16]. The schematic of the cylinder parameters is shown in Figure 8, and the displacement and pressure sensor arrangement is shown in Figure 9.

$$\dot{p}_A = \frac{1}{C_{HA}} \cdot (Q_A - Q_{Li} - A_A \cdot \dot{x}) \tag{17}$$

$$\dot{p}_B = \frac{1}{C_{HB}} \cdot (-Q_B + Q_{Li} + A_B \cdot \dot{x}) \tag{18}$$

where P_A, P_B are the cylinder chamber A and B pressure, bar; Q_A, Q_B are the cylinder chamber A and B flow rate, L/min; A_A, A_B are the cylinder bore and rod side annular area, m^2; x is the cylinder displacement, m; Q_{Li} is the leakage flow rate from chamber A to B; C_{HA}, C_{HB} are the hydraulic volume of chambers A and B, calculated by Equations (19)–(22).

$$Q_{Li} = k_{Li} \cdot (p_A - p_B) \tag{19}$$

$$C_{HA} = \frac{V_A}{K_{FL}},\ C_{HB} = \frac{V_B}{K_{FL}} \tag{20}$$

$$V_A = \left(\left[\frac{h}{2} + x \right] \cdot A_A + V_{LA} \right) \tag{21}$$

$$V_B = \left(\left[\frac{h}{2} - x \right] \cdot A_B + V_{LB} \right) \tag{22}$$

where k_{Li} is the flow rate leakage coefficient of chamber A to B; K_{FL} is fluid bulk modulus V_{LA}, V_{LB} are the chamber A and B dead zone volume.

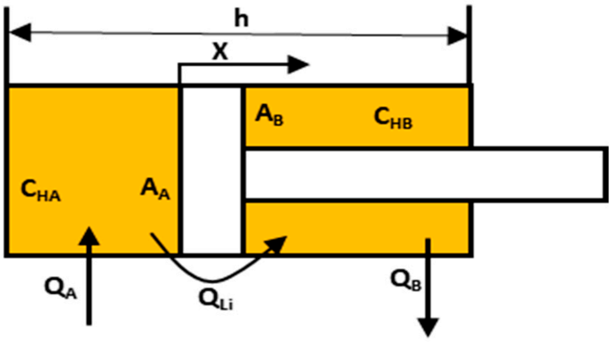

Figure 8. Schematic diagram of cylinder parameters.

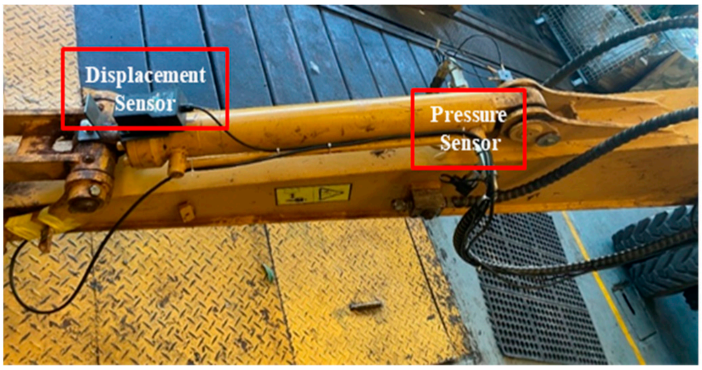

Figure 9. Installation position of cylinder displacement and pressure sensor.

In order to obtain sufficient operating data and ensure the consistency of each experiment, the experimental process and requirements are as follows:

1. Prepare two soil pits No. 1 and No. 2 at the experimental site, to ensure that the soil in the pits has a similar degree of looseness.

2. The excavator is operated by the same operator, its working speed is set to 1200 rpm.

3. During the operation, dig the original soil in the No. 1 pit and unloading it into the No. 2 pit.

4. Ensure that the duration of each cycle's operation and the duration of the same operation stages are similar, and the loading direction is changed after every 15 buckets.

5. Record the total number of buckets in the experiment for 15 min. The experimental process and the experimental site are shown in Figure 10.

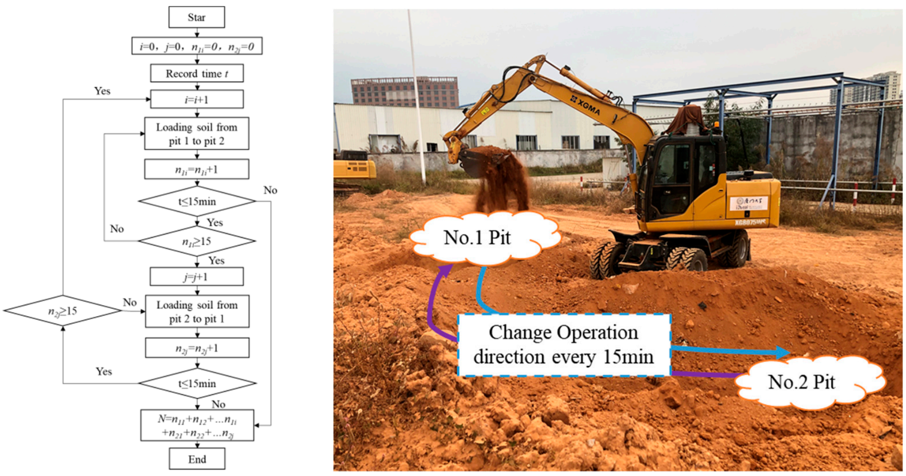

(**a**) (**b**)

Figure 10. Experimental process and test site. (**a**) Experimental process; (**b**) test site.

The experimental site for transportation conditions is a hard cement floor with a total length of 400 m. During the experiment, the engine speed was set at 2200 rpm, the gear was at the highest gear position, and the excavator was used for 30 cycles (12 km) without a load. Compared with the operation condition, the actuation system and the swing motor do not work in the transportation condition, and the data of the engine, torque converter, steering pump, and main pump are mainly collected. The collected data for transportation conditions are shown in Table 2.

Table 2. Data collection under transportation condition.

Serial Number	Components' Data	Serial Number	Components' Data
1	Main pump 1 outlet pressure	6	Main pump 2 outlet flow rate
2	Main pump 2 outlet pressure	7	Torque converter output speed
3	Steering pump outlet pressure	8	Torque converter output torque
4	Steering pump outlet flow rate	9	Engine output speed
5	Main pump 1 outlet flow rate	10	Engine output torque

3.2. Performance Data Acquisition

The excavator system theoretical energy analysis shows that the accurate energy flow analysis needs the components' performance data support. In this section, the component bench experiment to measure the hydraulic pumps and torque converter efficiencies is described. The main pump of the excavator is a variable displacement pump, and the steering pump is a fixed pump. Fixed pump efficiencies vary with loads, while variable displacement pump efficiencies vary with the loads and displacement ratios. The operating speed of the main pump and steering pump were set to 1200 rpm and their efficiencies were tested according to Standard JB/T7043. The test results are shown in Figure 11.

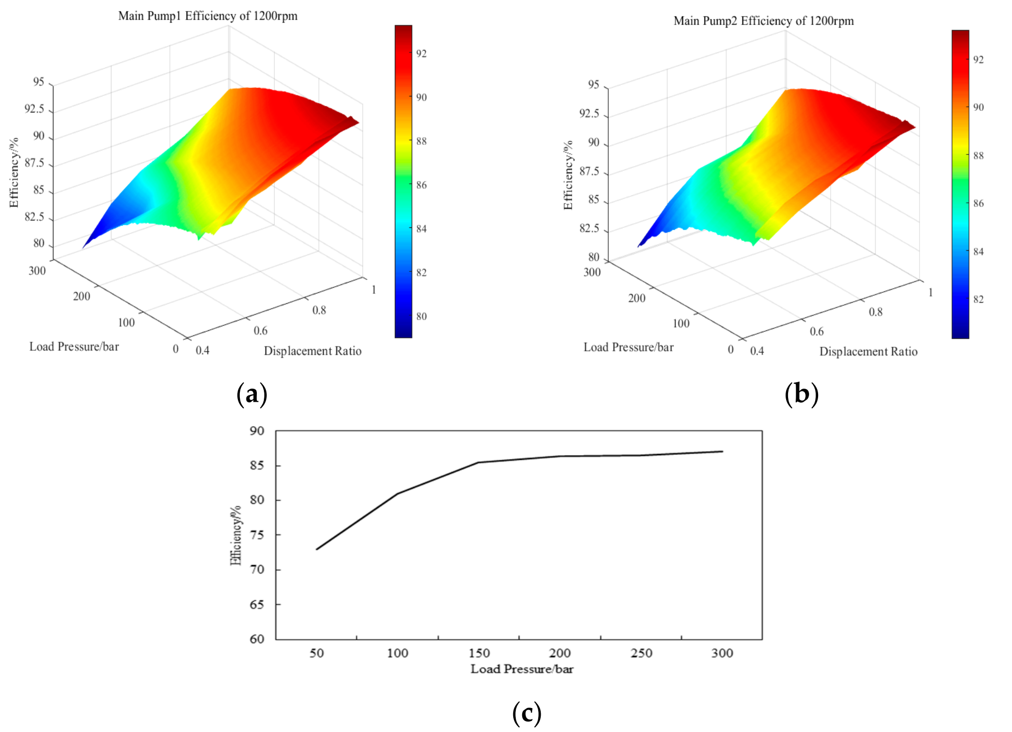

Figure 11. Efficiency results of hydraulic pumps at 1200 rpm. (**a**) Pump 1 displacement ratio-load-efficiency results; (**b**) pump 2 displacement ratio-load-efficiency results; (**c**) steering pump load-efficiency results.

The torque converter's efficiency test experiments were carried out. The experimental bench is shown in Figure 12a. The experimental steps are as follows:

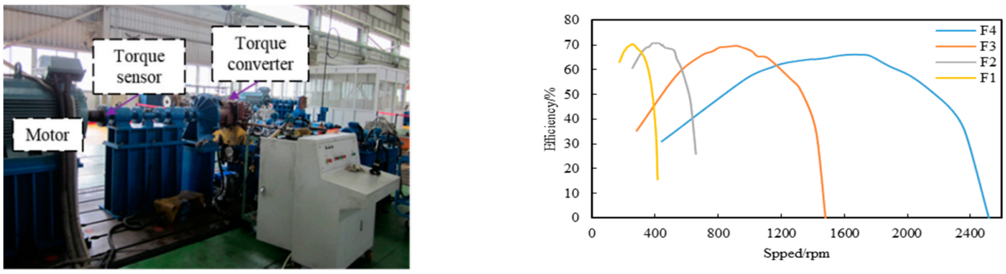

(**a**) (**b**)

Figure 12. Torque converter efficiencies test. (**a**) The torque converter efficiencies test bench; (**b**) the torque converter's efficiencies under different gear positions.

1. The motor simulates the output of the engine, keeps the input speed constant, and the experimental speed is set to 2200 r/min under the transport condition.

2. In the no-load state, increase the input speed to the set value. After the speed is stable, load successively at the output, reduce the output speed, and keep the input speed constant. After the loaded speed is fully stable, record the data.

3. The same experiment was repeated 5 times, and the average values of the 5 experiments were used as the experimental results.

According to the above experimental method, the efficiencies of the torque converter under different gear positions were measured, and the results are shown in Figure 12b.

4. System Energy Flow Analysis

4.1. Excavator Typical Working Condition Load Reconstruction

The wavelet decomposition method decomposes the excavator operation load into random and trend terms. The random term is processed by data segmentation, noise reduction, and singular value removal, and its stationarity is verified by the round-robin method. The random term's power spectrum is analyzed, and its parametric characterization is realized using the harmonic function method. The trend term is a non-stationary random signal. After the data segmentation, its mean square value is measured, and the load trend term is reconstructed by the weighted theory method. The reconstructed random and trend terms are combined, and the reconstruction of the typical condition load is complete. The process is shown in Figure 13.

As pump 2's load as an example, it is firstly decomposed into a random term and trend term through wavelet decomposition, then filtered and singular values are removed. The results are shown in Figure 14.

Its statistical characteristics are representative only when the load's random term is a stationary ergodic process of various states. The load random term of 60 cycles' operation data are divided into 10 subsample sequences of equal length. The mean square of each series is calculated and compared to the overall mean square of the random term. The round-robin method is used to carry out the ergodic process test of the stationary states [10], and the test results are shown in Table 3.

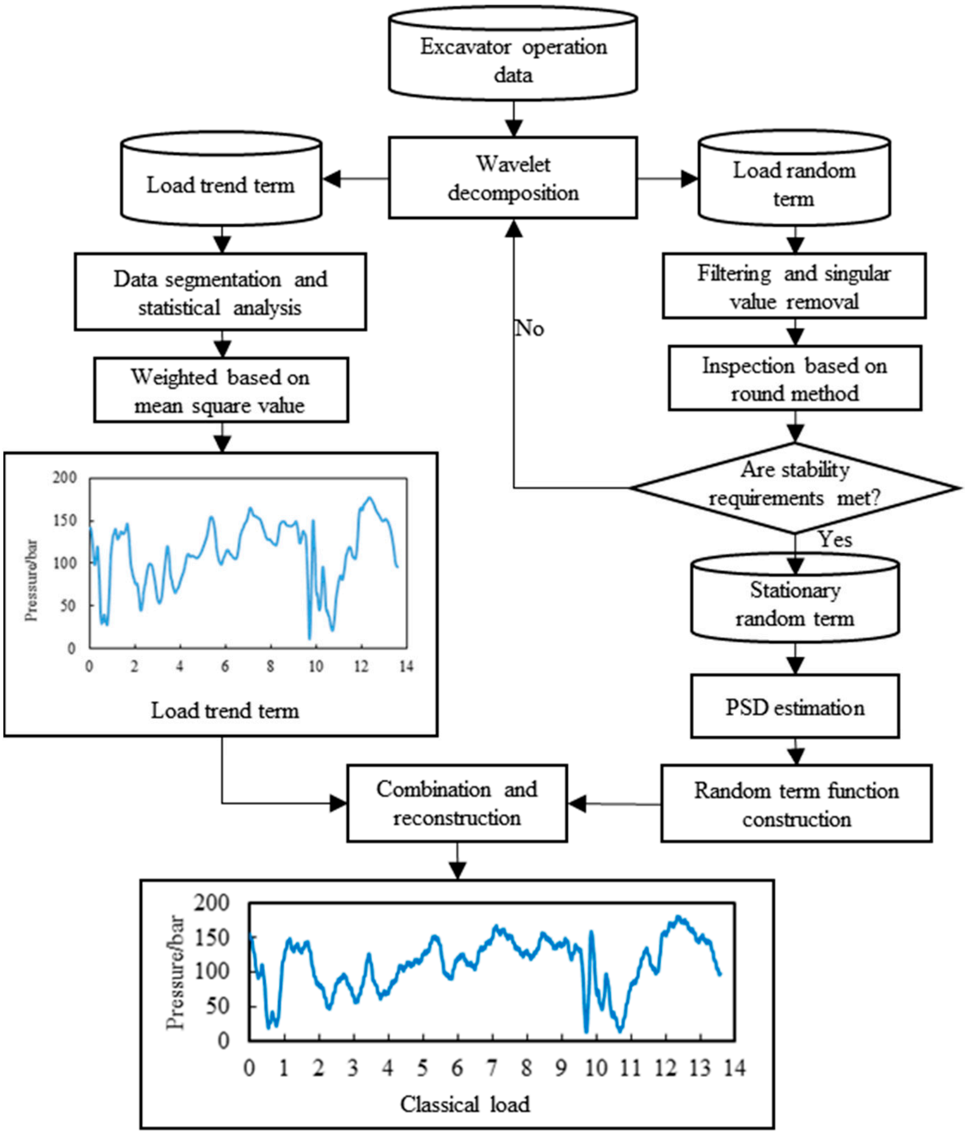

Figure 13. The typical working condition load reconstruction.

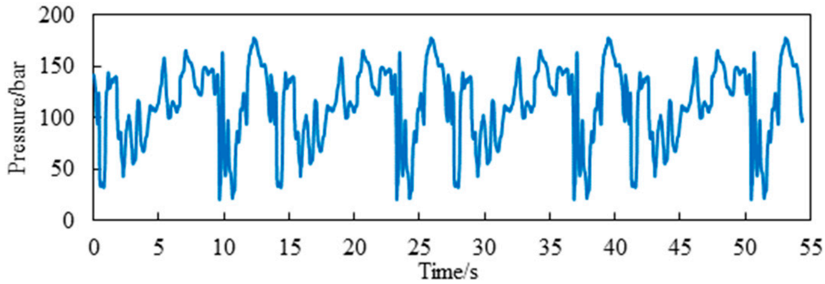

(**a**)

Figure 14. *Cont.*

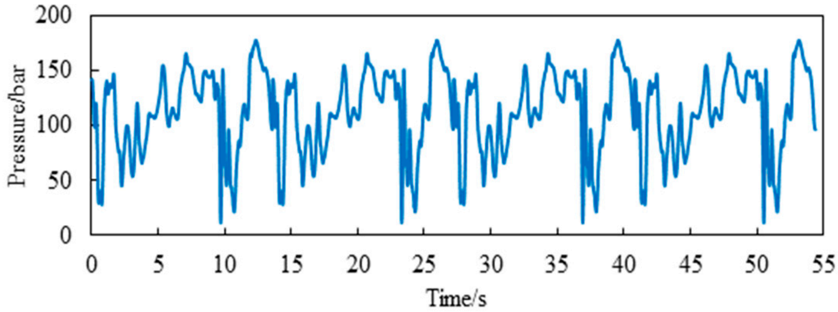

(**b**)

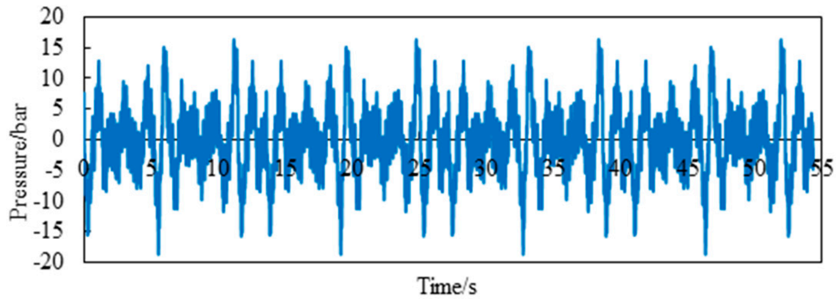

(**c**)

Figure 14. Wavelet decomposition results of main pump 2 in operation condition. (**a**) Original data; (**b**) trend term data; (**c**) random term data.

Table 3. Rounds statistics of load random term.

Serial Number	Mean Square Value	Rounds Statistics	Serial Number	Mean Square Value	Rounds
1	10.127	-	6	8.688	-
2	11.559	+	7	8.581	-
3	12.089	+	8	9.666	-
4	9.337	-	9	10.810	+
5	12.127	+	10	9.395	-
Total mean square value		10.316	Round numbers		6

When the number of subsamples is $n = 10$, under the significance level $\alpha = 0.05$, the number of rounds should be [3,8]. The number of statistical rounds of the load's random term is 6, so the assumption of stationarity is acceptable. If the samples of a random process are stationary and the experimental condition for obtaining each sample are basically the same, the stationary random process can be treated as an ergodic process.

Using the Welch method to estimate the power spectrum of the load's random term, the power spectral density function curve is shown in Figure 15. It can be seen from the figure that the load energy of the excavator's main pump 2 is concentrated in the range of 0 to 9 Hz, and there are two peak frequencies of 3.08 Hz and 4.02 Hz, which are consistent with the significant inertia of the excavator and its cyclic operation characteristics. The random load's power density spectrums are divided into several intervals according to the intermediate frequencies (the intermediate frequencies are $\omega_1, \omega_2, \ldots, \omega_n$), and the harmonic function approximation replaces the original random term at the discrete frequencies. Each harmonic component must satisfy the energy equivalence condition of Equation (23).

$$\frac{A_n^2}{2} = 2\int_{\omega_{n-1}}^{\omega_n} P(\omega)d(\omega) \tag{23}$$

where A_n^2 is the amplitude of the n_{th} harmonic function; $P(\omega)$ is the power spectral density of the random term.

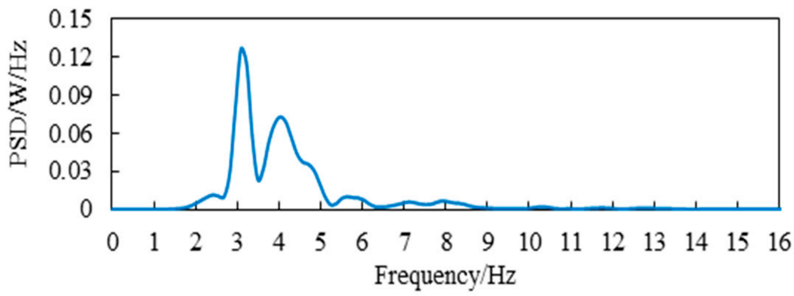

Figure 15. Power spectral density of load random term.

Combined with the results of the power spectral density of the load random term, the parameterization of the load random term is expressed as Equation (24). The parameterized expression of the load random term function is completed in the frequency range of 1 to 9 Hz. The accuracy of the reconstructed data can be evaluated by Formula (25), and the evaluation result R = 0.952, which proves that the reconstruction method has high accuracy. Figure 16 shows the comparison results of the reconstructed load's random term and the original load's random term.

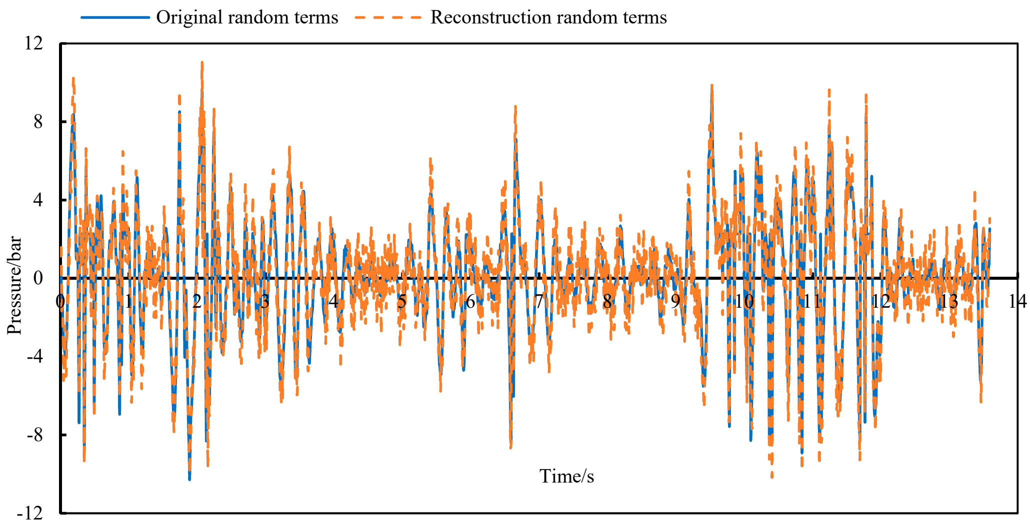

Figure 16. The comparison result between the reconstructed and original load random term.

$$f(t) = 2\sqrt{\int_{\omega_0}^{\omega_1} P(\omega)d\omega}\cos\left(\frac{\omega_1}{2}t + \varphi_1\right) + 2\sqrt{\int_{\omega_1}^{\omega_2} P(\omega)d\omega}\cos\left(\frac{\omega_1 + \omega_2}{2}t + \varphi_2\right) + \ldots 2\sqrt{\int_{\omega_{n-1}}^{\omega_n} P(\omega)d\omega}\cos\left(\frac{\omega_{n-1} + \omega_n}{2}t + \varphi_n\right) \quad (24)$$

$$R = 1 - \frac{\sum_{i=1}^{T} \frac{|P_{Ri} - P_{Oi}|}{P_{Oi}}}{T} \quad (25)$$

where P_{Ri} is the load random term after reconstruction; P_{Oi} is the original load random term; T is the total time of the sample.

Compared with the random term, the trend term cannot be parameterized by the harmonic function. Therefore, the trend term samples of 60 cycles' operation data are divided into 10 groups of subsamples, each group of subsamples has 6 operation segments of data, and each segment of operation segment data is divided into 5 operation stages. Based on the method from the literature [24], the divided operation sample data are theoretically weighted and reconstructed by Equations (26) and (27).

$$X_i = \sum_{j=1}^{10}\left(\frac{R_{ij}}{\sum\limits_{j=1}^{10} R_{ij}} x_{ij}\right)(i = 1, \ldots, 6;\ j = 1, \ldots, 10) \tag{26}$$

where i is the sequence number of the operation segment; j is the sequence number of the subsample; R_{ij} *is* the mean square value of the i_{th} operation segment of the j_{th} subsample; x_{ij} is the time domain waveform data of the i_{th} operation segment of the j_{th} subsample; X_i is the weighted data of the i_{th} operation segment.

$$y_i = \sum_{i=1}^{6}\left(\frac{R_{ik}}{\sum\limits_{k=1}^{6} R_{ik}} x_{ik}\right)(x_{ik} \in X_i)(i = 1, \ldots, 5;\ k = 1, \ldots, 6) \tag{27}$$

where k is the sequence number of the operation cycle; R_{ik} is the mean square value of the i_{th} operation stage of the k_{th} cycle; x_{ik} is the waveform data of the i_{th} operation stage of the k_{th} cycle; y_i is the weighted data of the i_{th} operation stage.

The result of the load's trend term after weighted reconstruction is shown in Figure 17. The operation conditions of the excavator include 5 stages of dig preparation, digging, lifting, unloading, and swinging. The boom and the swing system work in the stages of dig preparation, lifting, and swinging, so the load amplitude ranges in the three stages are close and smooth. During the digging stage, the bucket, boom, and stick work together, the load of the main pump is affected by the working resistance, and the load fluctuates greatly. During the dumping stage, where only the bucket works, there is a shock caused by load transients.

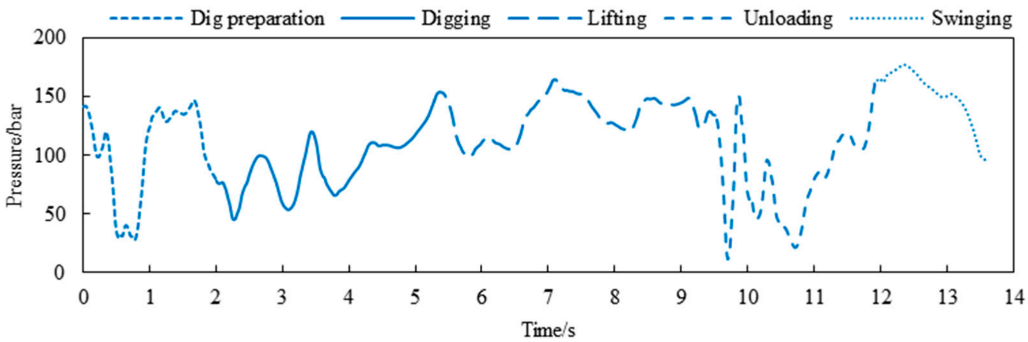

Figure 17. Reconstruction results of trend terms of typical load.

The load's random term is combined with the load's trend term to obtain the reconstructed load. The accuracy of the reconstructed data is evaluated by Equation (25), and the evaluation result R is 0.965, indicating that the accuracy of the reconstructed load is high, which proves that the load reconstruction method for typical working conditions is reasonable. The comparison result between the reconstructed load and the original load is shown in Figure 18.

Similarly, under transportation conditions, the output torque is decomposed into random and trend terms. The output torque is reconstructed by the harmonic function and the theoretical weighting method, and its evaluation result R is 0.973. The comparison results of the reconstructed output torque and the original torque are shown in Figure 19. Finally, the same method is used to reconstruct the typical working condition load of the main pump 1, boom, swing motor, engine, and other components. The energy flow analysis of the excavator under operation and transportation conditions is carried out based on typical working condition load.

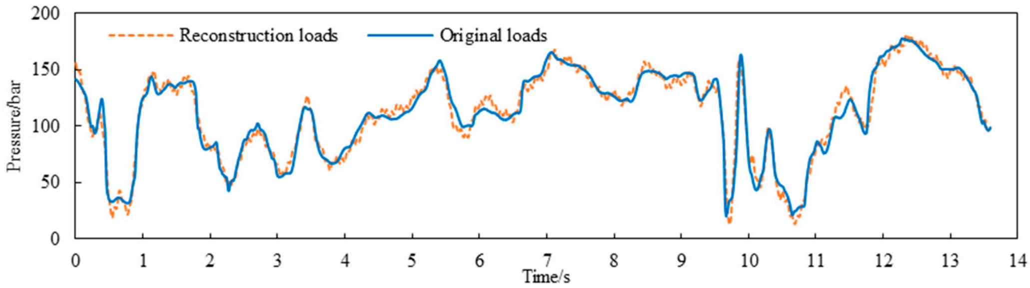

Figure 18. Comparison between reconstructed load and original data.

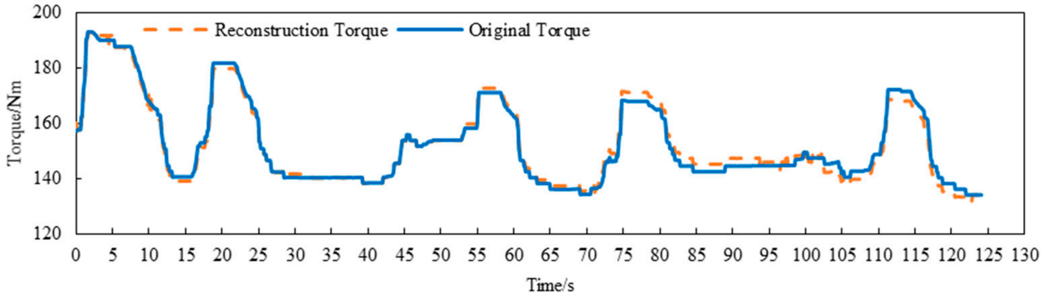

Figure 19. The comparison between reconstructed and original load.

4.2. Energy Flow Analysis Results

The results of the engine energy flow analysis are shown in Figure 20. The output energy of the engine only accounts for 50.21% of the engine's fuel energy, the heat loss accounts for 18.85% of the engine's fuel energy, and other consumption of the engine accounts for 30.94% of the engine's fuel energy.

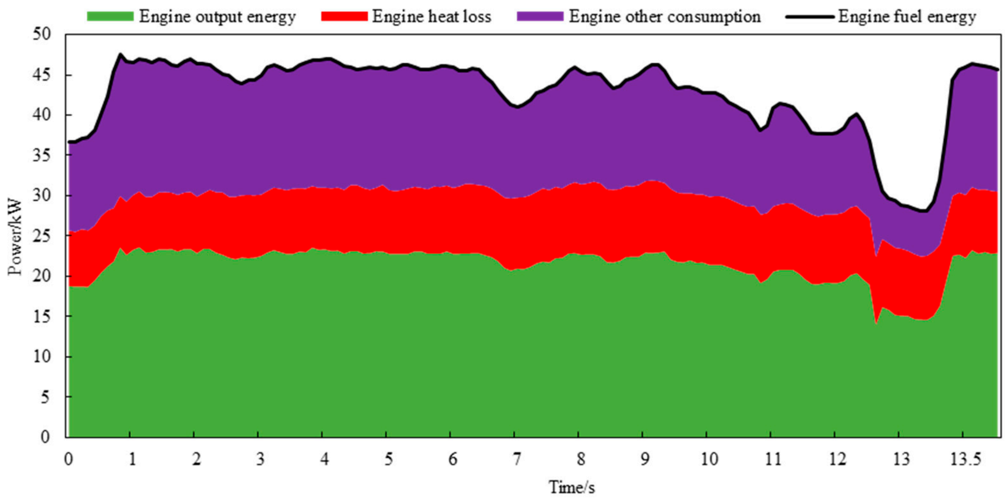

Figure 20. The engine energy flow.

The hydraulic pump energy flow analysis results are shown in Figure 21. The hydraulic pumps' efficiency loss, the hydraulic system's heat loss, the auxiliary components' consumption, and the hydraulic pumps' output energy account for 12.00%, 12.77%, 19.31%, and 55.92% of the engine's output energy, respectively.

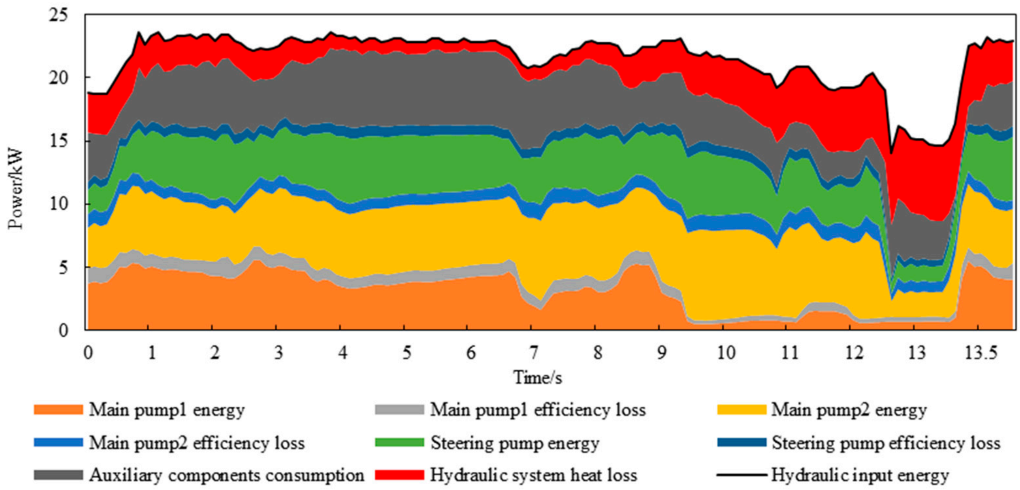

Figure 21. The hydraulic pump energy flow.

The energy flow analysis results of the operation system are shown in Figure 22. Motor consumption accounts for 14.23% of the system input energy. The boom, stick, and bucket work accounted for 11.09%, 3.46%, and 18.67% of the system input energy, respectively, totaling 33.22%. The loss in the hydraulic system circuit (cylinder loss, circuit loss, overflow loss, and main control valve loss) account for 52.55% of the system input energy. At the same time, in process of lowering the boom and stick, the gravitational potential energy released by itself is equivalent to 6.07% of the system input energy.

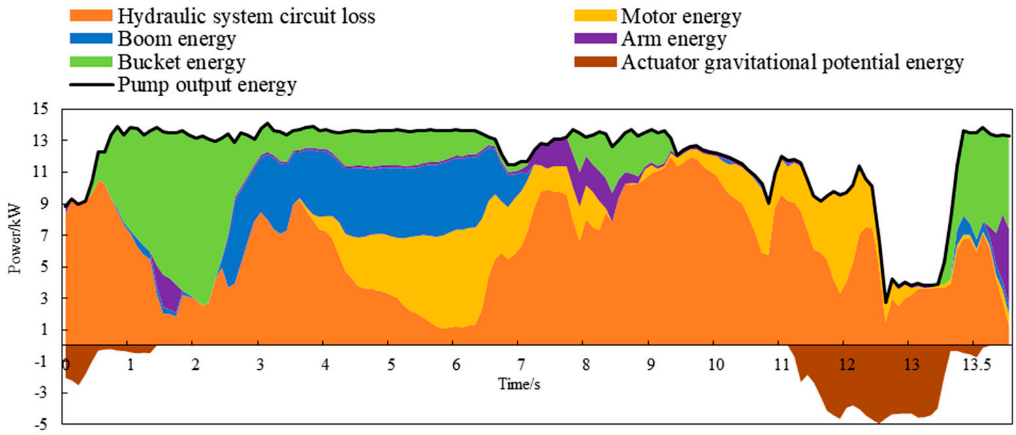

Figure 22. The operation system energy flow.

From each component's energy flow results, the proportion of component energy in the engine's fuel energy is further analyzed, and the energy flow in the excavator's one operation cycle is obtained. It can be seen from the analysis that the engine heat loss, engine other loss, and the engine's output energy account for 18.85%, 30.94%, and 50.21% of the engine's fuel energy, respectively. The hydraulic pump's efficiency loss, the hydraulic system's heat loss, the auxiliary components' consumption, and the hydraulic pump's output energy account for 6.03%, 6.41%, 9.69%, and 28.08% of the engine's fuel energy, respectively. The boom, stick, bucket, and swing motor energy consumption accounted for 3.11%, 0.98%, 5.24%, and 4.00% of the engine's fuel energy, respectively, totaling 9.33%. The hydraulic circuit system consumes 14.75% of the engine's fuel energy. In addition, during the lowering of the boom or stick, its gravitational potential energy is equivalent to 1.70% of the engine's fuel energy. The results are shown in Figure 23.

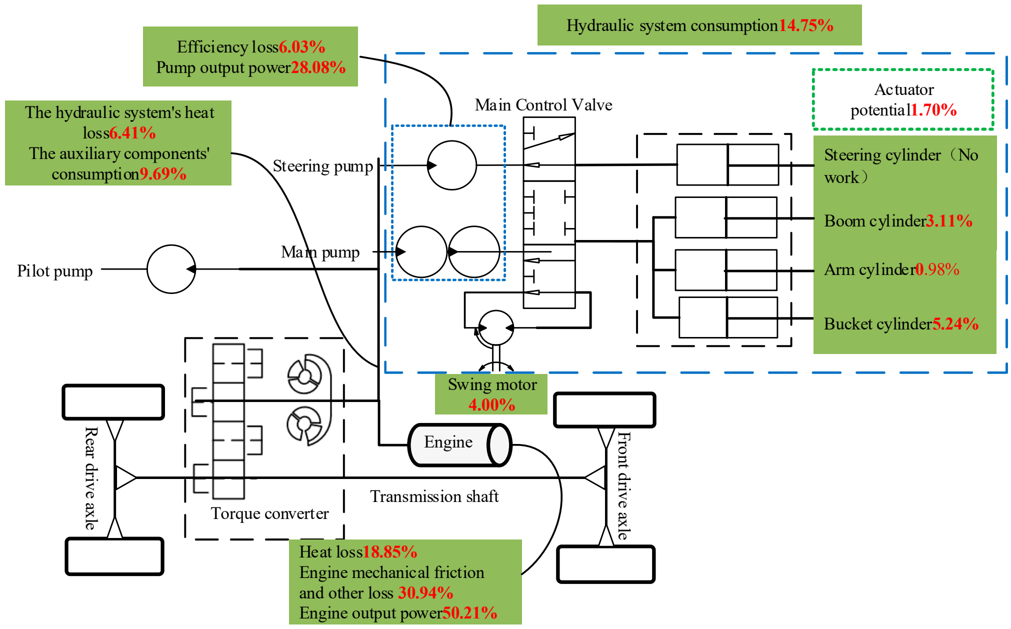

Figure 23. Excavator operation condition energy flow.

Under transportation conditions, the engine output energy, engine heat loss, and other loss account for 49.80%, 23.73%, and 26.47% of the engine's fuel energy. The main pump and steering pump consume 8.66% and 1.25% of the engine's fuel energy. The efficiency loss of the torque converter, the loss of the drive axle and wheel reducer, and the driving energy in transportation conditions account for 15.09%, 6.82%, and 17.98% of the engine fuel energy, respectively. The results are shown in Figure 24.

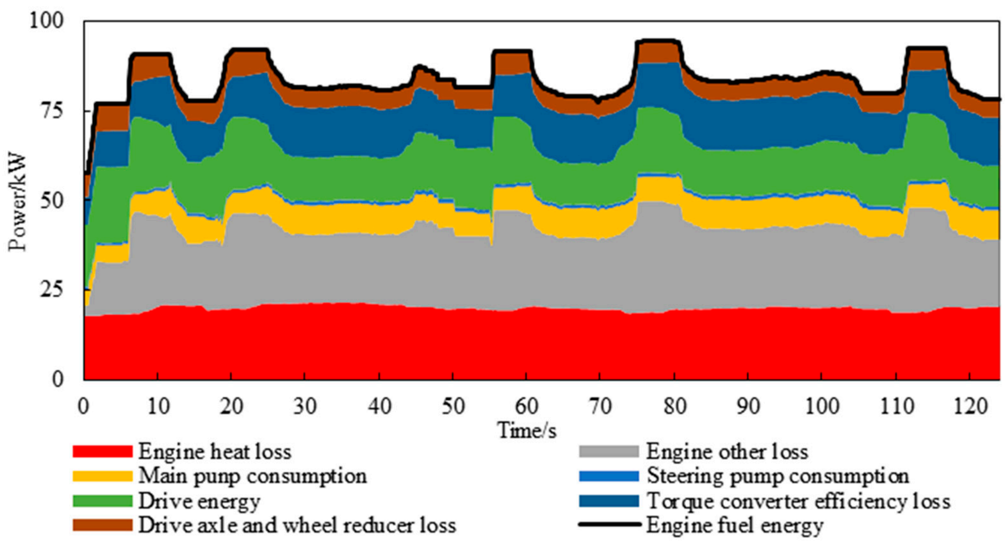

Figure 24. Transportation condition energy flow.

4.3. Experimental Verification

Ten experiments were carried out under operation and transportation conditions, the energy flow results based on the experimental data were obtained, and the average value was calculated. The comparison of energy flow analysis results based on typical working condition load and experimental data are shown in Tables 4–8. Under operation conditions, the maximum error between the two is 4.80%, and under transportation conditions, the maximum error between the two is 4.23%. The error of the energy flow analysis results of the two working conditions is less than 5%, which proves that the energy flow analysis method based on typical working conditions is reasonable.

Table 4. Engine energy flow results comparison under operation conditions.

Results	Fuel Energy	Heat Loss	Other Loss	Output Energy
Under typical condition load	46.26 kW	18.85%	30.94%	50.21%
Experimental results	48.53 kW	19.80%	30.99%	49.21%
Deviation	4.68%	4.80%	0.16%	2.03%

Table 5. Hydraulic pump energy flow results comparison under operation conditions.

Results	Output Energy	Hyraulic System Heat Loss and Auxiliary Components' Consumption	Efficiency Loss
Under typical condition load	28.08%	16.10%	6.03%
Experimental results	27.58%	15.70%	5.93%
Deviation	1.81%	2.55%	1.69%

Table 6. Operation system energy flow results comparison under operation conditions.

Results	Hydraulic System Consumption	Actuation System	Swing Motor	Regeneration of Actuators
Under typical condition load	14.75%	9.33%	4.00%	1.70%
Experimental results	13.98%	8.93%	3.82%	1.78%
Deviation	0.72%	4.48%	4.71%	4.49%

Table 7. Engine energy flow results comparison under transportation conditions.

Results	Fuel Energy	Heat Loss	Other Loss
Under typical condition load	84.05 kW	23.73%	26.47%
Experimental results	85.88 kW	24.05%	27.11%
Deviation	2.13%	1.33%	2.36%

Table 8. The transportation condition energy flow comparison results.

Results	Main Pump Consumption	Steering Pump Consumption	Torque Converter Efficiency Loss	Drive Axle and Wheel Reducer	Driving Energy
Under typical condition load	8.66%	1.25%	15.09%	6.82%	17.98%
Experimental results	8.36%	1.22%	14.95%	7.06%	17.25%
Deviation	3.59%	2.46%	0.94%	3.40%	4.23%

Whether it is operation or transportation conditions, the energy utilization rate of excavators is relatively low. Under the operation condition, the recoverable potential energy and the overflow loss of the swing process account for a large proportion. Reasonable energy recovery methods may be considered to recover it. Under transportation conditions, the main pump in the non-working state has a significant loss. Reducing the minimum output flow of the main pump may be considered, such as the use of a positive flow control pump.

5. Conclusions

In order to obtain accurate excavator energy flow results, this paper analyzes the excavator system's theoretical energy flow and obtains the excavator experimental data. The typical working condition load is reconstructed and the accurate analysis of the excavator energy flow is realized based on it. The work can be summarized as follows:

1. Data requirements are obtained according to the results of the system theoretical energy flow analysis, the experimental schemes are designed, and the excavator data are collected. The typical working condition load is reconstructed based on wavelet decomposition, harmonic function, and theoretical weighting methods, for which the accuracy evaluation value R is 0.965. The reconstructed load is close to the excavator's actual working condition load.

2. Under operation conditions, the output energy of the engine only accounts for 50.21% of the engine's fuel energy, and the energy consumption of the actuation and the swing system accounts for 9.33% and 4%, respectively. Under transportation conditions, the output energy of the engine only accounts for 49.80% of the engine's fuel energy, and the torque converter efficiency loss and excavator driving energy account for 15.09% and 17.98%, respectively. In both working conditions, the effective utilization rate of engine energy is low.

3. The energy flow analysis results provide energy margins for designing energy-saving schemes and control strategies. Energy recovery and reducing the main pump's minimum output flow rate can be considered for excavators' energy-saving control.

Author Contributions: Data collection experiments, D.S., X.B. and X.X.; Investigation, D.S.; Methodology, D.S., L.H. and S.W.; Writing—original draft, D.S.; Writing—review and editing, D.S., L.H. and S.W. All authors have read and agreed to the published version of the manuscript.

Funding: This project was supported by the National Key R&D Program of China (Grant No. 2020YFB1709901, No. 2020YFB1709904), National Natural Science Foundation of China (Grant No. 51975495, 51905460) and Guangdong Basic and Applied Basic Research Foundation (Grant No. 2021A1515012286).

Institutional Review Board Statement: The study did not require ethical approval.

Informed Consent Statement: The study did not involve humans.

Data Availability Statement: The study did not report any data.

Conflicts of Interest: The authors declare no conflict of interest.

References

1. Trani, M.L.; Bossi, B.; Gangolells, M.; Casals, M. Predicting fuel energy consumption during earthworks. *J. Clean. Prod.* **2016**, *112*, 3798–3809. [CrossRef]
2. Abekawa, T.; Tanikawa, Y.; Hirosawa, A. *Introduction of Komatsu Genuine Hydraulic Oil KOMHYDRO HE*; Komatsu Technical Report; Yumpu: Komatsu, Japan, 2010; Volume 56.
3. Ohira, S.; Suehiro, M.; Ota, K.; Kawamura, K. Use of emission rights for construction machinery to help prevent global warming. *Hitachi Rev.* **2013**, *62*, 123–130.
4. Yang, J.; Quan, L.; Yang, Y. Excavator energy-saving efficiency based on diesel engine cylinder deactivation technology. *Chin. J. Mech. Eng.* **2012**, *25*, 897–904. [CrossRef]
5. Xu, D.F. Analysis and Computing of Load Sensing System in Hydraulic Excavator. *J. Tongji Univ.* **2001**, *29*, 1097–1100.
6. Gao, F.; Pan, S.X. Experimental study on model of negative control of hydraulic system. *J. Mech. Eng.* **2005**, *41*, 107–111. [CrossRef]
7. Ge, L.; Dong, Z.; Quan, L.; Li, Y. Potential energy regeneration method and its engineering applications in large-scale excavators. *Energy Convers. Manag.* **2019**, *195*, 1309–1318. [CrossRef]
8. Choi, K.; Seo, J.; Nam, Y.; Kim, K.U. Energy-saving in excavators with application of independent metering valve. *J. Mech. Sci. Technol.* **2015**, *29*, 387–395. [CrossRef]
9. Zhang, J.; Li, K.; Guan, L.; Zhu, T. Research on Positive Control System with Synthetic Pilot Pressure of Excavator. *China Mech. Eng.* **2012**, *23*, 1537–1541. [CrossRef]
10. Kim, Y.; Kim, P.; Murrenhoff, H. Boom potential energy regeneration scheme for hydraulic excavators. In Proceedings of the ASME/BATH 2016 Symposium on Fluid power and Motion Control, Bath, UK, 7–9 September 2016.
11. Zhao, P.; Chen, Y.; Zhou, H. Simulation analysis of potential energy recovery system of hydraulic hybrid excavator. *Int. J. Precis. Eng. Manuf.* **2017**, *18*, 1575–1589. [CrossRef]
12. Xiao, Q.; Wang, Q.; Zhang, Y. Control strategies of power system in hybrid hydraulic excavator. *Autom. Constr.* **2008**, *4*, 361–367. [CrossRef]

13. Kwon, T.S.; Lee, S.W.; Sul, S.K.; Park, C.G.; Kim, N.I.; Kang, B.I.; Hong, M.S. Power Control Alg-orithm for Hybrid Excavator with Supercapacitor. *IEEE Trans. Ndustry Appl.* **2010**, *46*, 1447–1455. [CrossRef]
14. Deppen, T.O.; Alleyne, A.G.; Stelson, K.; Meyer, J. A model predictive control approach for a parallel hydraulic hybrid powertrain. In Proceedings of the American Control Conference, San Francisco, CA, USA, 29 June–1 July 2011; IEEE: Piscataway, NJ, USA; pp. 2713–2718.
15. Shen, W.; Jiang, J.; Su, X.; Karimi, H.R. Energy-saving analysis of hydraulic hybrid excavator based oncommon pressure rail. *Sci. World J.* **2013**, *2013*, 560694. [CrossRef] [PubMed]
16. Zimmerman, J.D.; Pelosi, M.; Williamson, C.A. Energy consumption of an LS excavator hydraulic system. In Proceedings of the ASME International Mechanical Engineering Congress and Exposition, Seattle, WA, USA, 11–15 November 2007; pp. 117–126.
17. Casoli, P.; Riccò, L.; Campanini, F.; Lettini, A.; Dolcin, C. Mathematical model of a hydraulic excavator forfuel consumption predictions. In Proceedings of the ASME/BATH 2015 symposium on Fluid Power and Motion Control, Chicago, IL, USA, 12–14 October 2015.
18. Altare, G.; Padovani, D.; Nervegna, N. A Commercial Excavator: Analysis, Modelling and Simulation of theHydraulic Circuit. In Proceedings of the SAE 2012 Commercial Vehicle Engineering congress, Rosemont, IL, USA, 13–14 September 2012.
19. Casoli, P.; Riccò, L.; Campanini, F.; Bedotti, A. Hydraulic hybrid excavator—Mathematical model validationand energy analysis. *Energies* **2016**, *9*, 1002. [CrossRef]
20. Bedotti, A.; Campanini, F.; Pastori, M.; Riccò, L.; Casoli, P. Energy saving solutions for a hydraulic excavator. *Energy Procedia* **2017**, *126*, 1099–1106. [CrossRef]
21. An, K.; Kang, H.; An, Y.; Park, J.; Lee, J. Methodology of excavator system energy flow-down. *Energies* **2020**, *13*, 951. [CrossRef]
22. Zhai, X.; Wang, J.; Chen, J. Parameter Estimation Method of Mixture Distribution for Construction Machinery. *Math. Probl. Eng.* **2018**, *2018*, 3124048. [CrossRef]
23. Zhai, X.; Zhang, X.; Jiang, Z.; Li, Y.; Zhang, Q.; Wang, J. Load spectrum compiling for wheel loader semi-axle based on mixed distribution. *Trans. Chin. Soc. Agric. Eng. (Trans. CSAE)* **2018**, *34*, 78–84.
24. Chang, L.; Xu, L.; Lü, M.; Liu, Y.; Zhao, Y. Driving cycle construction of loader based on typical working condition test. *Trans. Chin. Soc. Agric. Eng. (Trans. CSAE)* **2018**, *34*, 63–69.
25. Jiang, T.; Fu, Z.Y.; Wang, A.L. Parameterized load model under non-stationary random cyclic conditions. *J. Northeast. Univ. (Nat. Sci.)* **2016**, *37*, 845–850.
26. Chen, Y.; Wang, A.; Li, X. Load Classification Design of Excavator Multiway Valve. *J. Xi′an Jiaotong Univ.* **2020**, *54*, 100–108.
27. Peng, B. Research on Stage-Based Power Matching Control of Hydraulic Excavator. Ph.D. Thesis, ZheJiang University, Hangzhou, China, 2016.
28. Wang, S.J.; Hou, L.; Huang, H.T.; Zhu, Q. Application of optimal shift control strategy on human intelligent fuzzy control. *J. Xiamen Univ. (Nat. Sci.)* **2016**, *55*, 131–136. (In Chinese)